JCTC Journal of Chemical Theory and Computation

Computational Characterization of Metal Binding Groups for Metalloenzyme Inhibitors

Kerwin D. Dobbs,[†] Amy M. Rinehart,[†] Michael H. Howard, Ya-Jun Zheng,* and Daniel A. Kleier*

DuPont Crop Protection, Stine-Haskell Research Center, P.O. Box 30, Newark, Delaware 19714

Received August 3, 2005

Abstract: The mode of action of many pest or disease control agents involves inhibition of some metalloenzyme that is essential for the survival of the target organism. These inhibitors typically consist of a functional group that is capable of a primary binding interaction with the metal and a scaffold that is capable of secondary interactions with the remainder of the enzyme. To characterize the binding ability of various metal binding groups (BGs), we have performed electronic structure calculations on ligand displacement reactions in a model system related to the metalloenzyme, peptide deformylase: $E-M-R + BG \rightarrow E-M-BG + R$. Here E represents a model coordination environment for the metal M, and R is a reference ligand (e.g., water) that may be displaced by a metal binding group. Since the oxidation state of many of the metals considered allows for multiple spin states, we also studied the influence of spin state on the coordination environment. Qualitative considerations of electronic structure inspired by the calculations provide an understanding of binding energy trends across a variety of ligands for a given metal and across a variety of metals for a given ligand.

Introduction

Many biologically active molecules act by binding to a metal ion. Some act as ionophores by transporting metals across membranes.[1] Others act as inhibitors of metalloenzymes by binding a metal at the active site.[2−6] In this report we describe the application of electronic structure calculations to study metal binding in model systems related to metalloenzymes such as peptide deformylase (PDF). PDF catalyzes the deformylation of the initial methionine of a nascent polypeptide and is a validated target for both antibiotics[7] and herbicides.[8] Crystal structures have been reported for the *E. coli*[9] enzyme containing three different metal cofactors Fe(II),[9,10] Ni(II),[9,11,12] and Zn(II)[9] and a variety of metal coordinating ligands including water,[9] the tripeptide, Met-Ala-Ser,[9] hydroxamic acids such as β-sulfonyl- and β-sulfinylhydroxamic acids,[11] and actinonin[12,10] as well as carboxylates exemplified by matlystatin analogues.[10]

We have been interested in designing selective PDF inhibitors as herbicides.[13,14] To facilitate such a design effort, a better understanding of the nature of the interaction between metal center and the metal binding group of a potential inhibitor is critical. A close-up view of the active site of Zn−PDF[9] from *E. coli* is illustrated in Figure 1. The enzyme contributes three ligands to the tetrahedral coordination sphere of the zinc: two histidines and a cysteine. The fourth ligand in this structure is a water molecule.

The calculations reported below address structural and spin state preferences for a simplified model of the active site of PDF in which the three amino acid residues are replaced by a tridentate ligand. These preferences are assessed as a function of metal type (Fe(II), Co(II) and Ni(II), Zn(II)). In addition, we evaluate the ability of other metal binding groups to displace the water from the model structures.

---

* Corresponding authors e-mail: YA-JUN.ZHENG@USA.dupont.com (Y.-J.Z.); e-mail: daniel.kleier@drexel.edu (D.A.K.) and phone: (215)895-1861. Corresponding author address: Department of Chemistry, Drexel University, Disque Hall, Room 305, 3141 Chestnut Street, Philadelphia, PA 19104-2875 (D.A.K.).

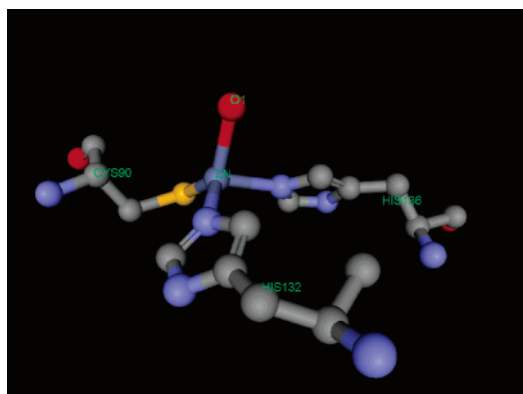† Current address: DuPont Central Research and Development, Wilmington, DE.

Computational Characterization of Metal Binding Groups

J. Chem. Theory Comput., Vol. 2, No. 4, 2006 **991**

Figure 1. Detail of active site of Zn(II)PDF according to Becker and co-workers.[9]
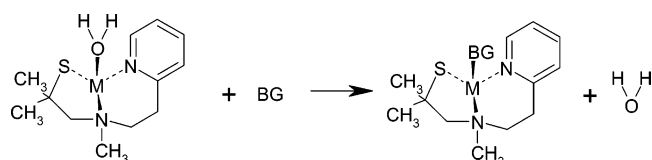

Figure 2. Water displacement reaction used to rank coordinating ability of binding groups, BG.

Methods

To rank order the coordinating ability of metal binding groups (BGs) we performed a series of computational studies of their ability to displace water from the complex shown in Figure 2. The complex consisted of a metal dication (iron-(II), cobalt (II), nickel(II), or zinc(II)) wrapped in a tridentate spectator ligand 2-methyl-1-([methyl-(2-pyridin-2-ylethyl)-amino]propane-2-thiolate, referred to as PATH for short. We chose the PATH ligand as our model system not only for reasons of computational efficiency but also because of its promotion[15] as a good structural mimic of the (His)(His)-(Cys) triad at the active site of metalloenzymes such as PDF and because direct comparison with experiment was possible.[15]

Density functional methods have been the method of choice for many modeling studies of metalloenzymes.[10] All calculations reported in this paper were performed with the density functional theory (DFT) methods as implemented within the Gaussian 03 suite of programs.[16] Each molecular structure was first optimized using the BP86/DGDZVP method. The optimized structure was then used in subsequent analytic vibrational frequency calculations at this same level of computation in order to ensure that the structure was indeed at a minimum on the potential energy surface. The pure BP86 functional[17,18] was chosen mainly because of its enhanced performance for optimization and vibrational frequency calculations compared to B3LYP.[19] Pure functionals are able to take advantage of using density fitting basis sets which expand the density in a set of atom-centered functions when computing the Coulomb interaction instead of computing all of the two-electron integrals.[20] DGDZVP basis sets[21] are all-electron, double-ζ valence polarized basis sets which were optimized specifically for DFT methods.

From the outset of this study, we initially used the B3LYP functional for binding energy analysis, since no generally accepted protocols for transition-metal reaction energetics

had been reported in the literature[22] at the time we began this study, and the B3LYP functional was known to do very well for the main group reactions.[23] The extensive experience of one of the authors (K.D.D.) with many different main group and organometallic systems led to the conclusion that differences between BP86 and B3LYP structures are minor while using the DGDZVP basis sets.[24] Building on this same experience, the reaction entropy, enthalpy, and free energy values reported below were determined from B3LYP/DGDZVP single-point energies on BP86/DGDZVP optimized structures in combination with the zero-point energy and vibrational thermal corrections (at 298.15 K) obtained from the BP86/DGDZVP vibrational frequencies. This same protocol was also used for determining the free energy differences, ΔG, between high- and low-spin states for (PATH)M(II)Br complexes in Table 1.

Results

Influence of Spin on Conformation of Coordination Sphere. The arrangement of ligands around the metal in the crystal structures of the Fe, Ni, and Zn forms of PDF is roughly tetrahedral in nature. A similar arrangement is observed in the crystal structures of the model (PATH)M-(II)(BG) complexes,[15] one of which is illustrated in Figure 3. In the model complexes the sulfide, tertiary amine nitrogen, and pyridine nitrogen serve as surrogates for the corresponding atoms in the cysteine and a pair of histidine residues of the PDF active site (see Figure 1).

As shown in Table 1, our DFT calculations found the arrangement of ligands in the model (PATH)M(II)Br systems to be spin dependent. When the geometries of the high-spin states were optimized, a rough tetrahedral arrangement of ligands was generally found. In the low-spin states the optimized structures are better described as square planar. Table 1 also presents the energy difference between high- and low-spin states for (PATH)M(II)Br complexes. The high-spin tetrahedral conformation is favored according to the calculations for all the (PATH)M(II)Br complexes but only by a relatively modest 6.7 kcal/mol for the Ni(II) complex. Thus, it is, perhaps, not too surprising that a recent crystallographic investigation has revealed square planar Ni-(II) centers in the *dimer* of (PATH)Ni(II)Br.[15d] On the other hand, spectroscopic evidence for the (PATH)Co(II)Br complex supports a high-spin tetrahedral ground state[15] consistent with predictions of the calculations.

The structures of the optimized quartet and doublet (PATH)Co(II)Br complexes are illustrated in Figure 4. The quartet state optimized to the cis diastereomer in which the N$-$CH$_3$ and bromide are on the same side of the fused 5,6-membered chelate ring system. Both the *N*-methyl and bromide groups are pointing toward the reader in Figure 4. In addition to a flatter arrangement of ligands about the cobalt, the optimized doublet structure has shorter bonds between the metal and the pyridine (N$_1$) and tertiary amine (N$_2$) nitrogens ($d[\text{N}_1-\text{Co}] = 1.96$ Å, $d[\text{N}_2-\text{Co}] = 2.03$ Å) as compared with the tetrahedral quartet structure ($d[\text{N}_1-\text{Co}] = 2.01$ Å, $d[\text{N}_2-\text{Co}] = 2.13$ Å).

Calculated geometric parameters for the high-spin (PATH)Co(II)Br and (PATH)Zn(II)Br complexes are compared with

992 *J. Chem. Theory Comput., Vol. 2, No. 4, 2006*

Dobbs et al.

Table 1. Arrangement of Ligands and Relative Free Energies, ΔG, of DFT Optimized Geometries for (PATH)M(II)Br Complexes in High- and Low-Spin States

metal	assigned multiplicity	optimized geometry	assigned multiplicity	optimized geometry	ΔG (high spin $-$ low spin) kcal/mol
Fe(II)	quintet	tetrahedral	triplet	square planar	−18.5
Co(II)	quartet	tetrahedral	doublet	square planar	−16.6
Ni(II)	triplet	tetrahedral	singlet	square planar	−6.7
Zn(II)	singlet	tetrahedral			
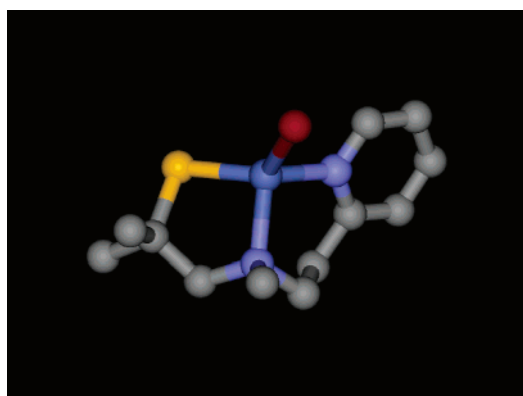
Figure 3. Crystal structure of (PATH)CoBr from Chang et al.[15] The positions of the hydrogen atoms have been suppressed for clarity.
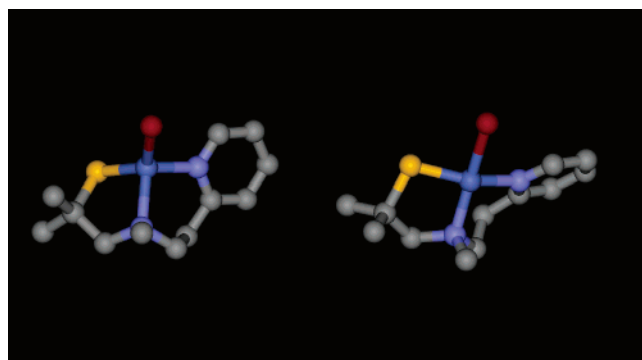
Figure 4. Comparison of optimized geometries for quartet (left) and doublet (right) (PATH)Co(II)Br.

Table 2. Calculated and Experimental Geometric Parameters for Quartet (PATH)Co(II)Br[a]

bond length	calcd	exptl	bond angle	calcd	exptl
Co−N$_1$	2.01	2.04	S−Co−N$_2$	91.1	91.9
Co−N$_2$	2.13	2.09	N$_1$−Co−N$_2$	101.0	100.2
Co−S	2.20	2.23	N$_1$−Co−Br	108.9	103.5
Co−Br	2.36	2.38	N$_2$−Co−Br	113.8	116.4
			S−Co−N$_1$	112.0	119.7
			S−Co−Br	126.3	122.9

[a] In this table N1 refers to the nitrogen of the pyridine ring, and N2 is the tertiary amine nitrogen.

those reported for the crystal structures in Tables 2 and 3, respectively. Key trends for distances and angles that involve the metal seem to be captured by the calculations (e.g., the ordering of bond distances and bond angles). The greatest discrepancies are the 8° difference for the S−Co−N$_1$ bond angle in the Co complex and the 12° difference in the S−Zn−Br angle in the Zn complex. Examination of the

Table 3: Calculated and Experimental[15b] Geometric Parameters for (PATH)Zn(II)Br[a]
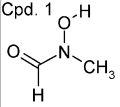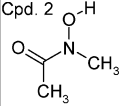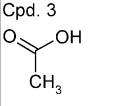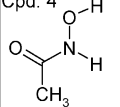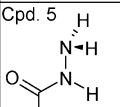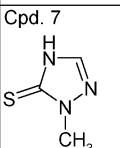
bond length	calcd	exptl	bond angle	calcd	exptl
Zn−N$_1$	2.13	2.06	S−Zn−N$_2$	90.2	92.9
Zn−N$_2$	2.23	2.11	N$_1$−Zn−N$_2$	96.7	99.3
Zn−S	2.28	2.26	N$_1$−Zn−Br	102.0	102.2
Zn−Br	2.39	2.38	N$_2$−Zn−Br	112.0	116.0
			S−Zn−N$_1$	113.9	120.9
			S−Zn−Br	135.2	123.3

[a] In this table N1 refers to the nitrogen of the pyridine ring, and N2 is the tertiary amine nitrogen.

calculated geometry revealed that the optimized conformation of the folded 5,6-membered chelate ring system is quite similar to that observed in the crystal structure. This conformational similarity can be appreciated by comparing the quartet structure on the left-hand side of Figure 4 with the experimental structure appearing in Figure 3. The conformation of the six-membered chelate ring in both the experimental and the optimized structure is a twist boat with the Co and an opposing methylene at the bowsprits. In both structures the conformation of the five-membered chelate ring places the exo methyl in an axial orientation and relatively close to the *N*-methyl group. It should be noted that at least one other energetically accessible conformation was discovered during the course of this work for the folded 5,6-membered chelate ring system. In this conformation the six-membered ring is closer to an idealized boat, while the five-membered ring assumes a conformation that places the exo methyl group in an equatorial orientation. Depending somewhat on the fourth ligand, this alternative conformation is calculated to be 3−4 kcal/mol higher in energy.

Metal Chelating Ability of Alternative Metal Binding Groups. Hydroxamic acids[5,11] and *N*-acylhydroxylamines[12] have been the metal binding groups of choice for peptide deformylase inhibitors. We sought to understand the potential for alternative functional groups to substitute for hydroxamic acids by examining the optimized structures of their complexes with the metals in the model coordination systems and comparing computed enthalpies for the water displacement reaction shown in Figure 2. The water displacement calculations were performed on the high-spin complexes, since the tetrahedral geometries realized for this spin state are more representative of the coordination sphere observed by X-ray crystallography for both the (PATH)M(II)Br complexes and the active site of PDF. The 5- and 6-membered chelate rings maintained the optimized conformation described above for the (PATH)Co(II)Br high-spin complex.

Computational Characterization of Metal Binding Groups

J. Chem. Theory Comput., Vol. 2, No. 4, 2006 **993**

Table 4. Calculated Thermodynamic Parameters for Displacement of Water from (PATH)M(II)(H$_2$O) Complexes by Various Metal Binding Groups (MBGs)[a]

Metal→	Fe			Co			Ni			Zn		
Binding Group ↓	ΔS	ΔH	ΔG	ΔS	ΔH	ΔG	ΔS	ΔH	ΔG	ΔS	ΔH	ΔG
Cpd. 1	-10.1	-12.7	-9.7	-12.0	-12.8	-9.2	-12.4	-9.8	-6.0	-12.7	-13.1	-9.3
Cpd. 2	-6.6	-13.7	-11.8	-10.1	-14.2	-11.2	-11.0	-11.3	-8.1	-11.6	-14.1	-10.7
Cpd. 3	-1.7	0.0	0.5	-5.5	-0.6	1.0	-5.5	0.0	1.6	-4.5	0.1	1.4
Cpd. 4	-6.1	-13.0	-11.2	-9.4	-13.5	-10.7	-6.8	-10.8	-8.8	-9.6	-13.6	-10.7
Cpd. 5	-10.1	-15.0	-12.0	-9.8	-13.7	-10.8	-13.8	-13.9	-9.8	-9.1	-13.0	-10.3
Cpd. 6	-4.6	2.2	3.6	-6.2	1.8	3.7	-6.0	2.6	4.4	-5.7	2.3	4.0
Cpd. 7	-9.7	-17.0	-14.1	-8.8	-17.8	-15.2	-9.7	-15.2	-12.3	-11.6	-19.5	-16.0

[a] Entropy changes are in cal/mol. Enthalpy and free energy changes calculated at 298 K are in kcal/mol.

Calculated binding energies and entropies relative to water are presented in Table 4, and binding enthalpies are plotted as a function of metal in Figure 5. Of the four metals considered, binding is generally weakest to the (PATH)Ni-(II) complex and similar in strength for coordination to the other three metals. Of the neutral complexes considered, the thiotriazolinone (compound 7 plotted in orange) generally binds best to all (PATH)M(II) complexes, followed closely by the *N*-acetylhydrazine (compound 5 in green), the *N*-acetylhydroxylamine (compound 4 in red), and the *N*-acyl,*N*-methylhydroxylamines (compounds 1 and 2 in blue and black, respectively).

Although neutral acetic acid is not predicted to be a particularly strong binder, the anion is a different story. It is off scale because of the strongly stabilizing electrostatic interaction with the positively charged metal. It will be necessary to take account of desolvation in order to reliably compare such anionic binding groups with the neutral ones described here.

Examination of the optimized structures for the *N*-acylhydroxylamine and hydroxamic acid complexes revealed some unexpected results. Instead of bidentate chelation of the metal as observed in PDF cocrystals with ligands of this type, the calculations predict a single dative bond between the carbonyl oxygen of the binding group and the metal of the model system. Instead of forming the expected second dative bond with the metal, the hydroxyl group of these ligands spun around the N−O axis to donate a hydrogen bond to the nearby negatively charged sulfide of the PATH ligand (See Figure 6). Interestingly, a bidentate interaction with the metal is realized for the (PATH)Fe(II)(*N*-acetylhy-drazine) complex as shown in Figure 7 but at the expense of losing the hydrogen bond with the sulfide.
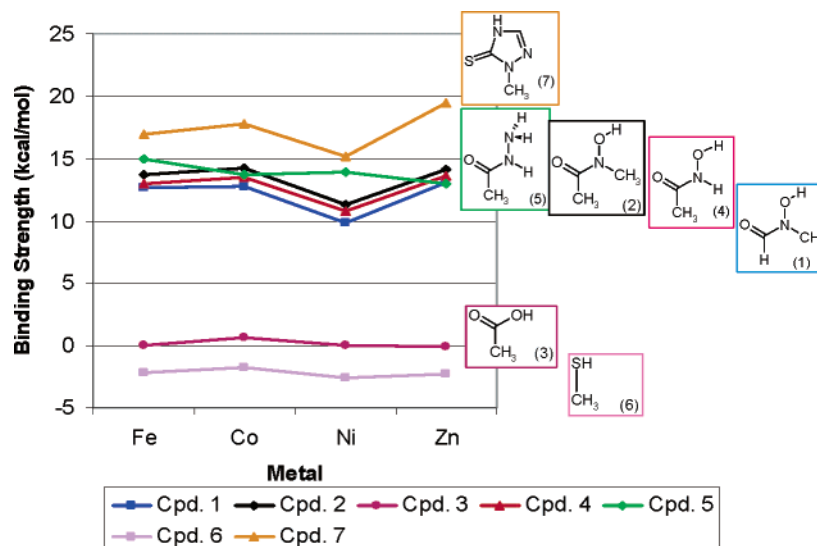
Figure 5. Binding strength ($-\Delta H$ for water displacement) for neutral binding groups as a function of metal.
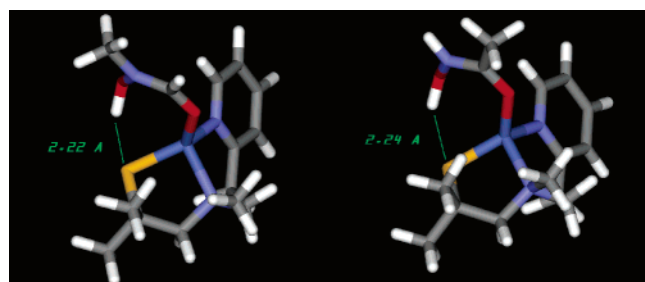

Figure 6. Optimized structures illustrating hydrogen bonding for (PATH)Co(II)(*N*-formyl,*N*-methylhydroxylamine) (compound 1, left) and *N*-acetylhydroxylamine (compound 4, right).
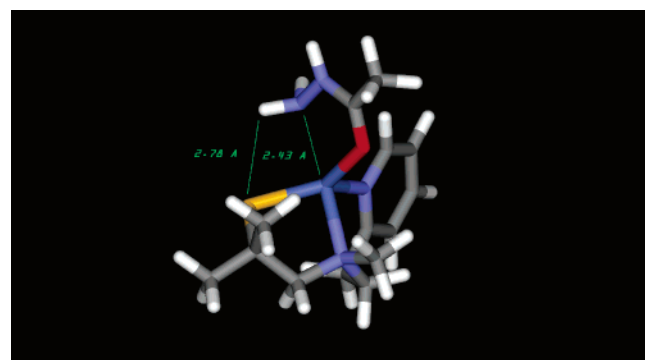

Figure 7. Optimized structure for (PATH)Fe(*N*-acetylhydrazine) complex. Bond distances shown in green are in angstroms. Bond distance to iron from the carbonyl oxygen of ligand is 2.12 Å.

Discussion

Geometries and Spin States. The general agreement between the calculated and experimentally determined geometries of the (PATH)M(II)Br complexes (Tables 2 and 3, Figures 3 and 4 left) builds confidence in the calculated binding trends reported here. Many of the predictions are also supported by qualitative considerations of molecular orbital intereactions. For example, the preference for a roughly tetrahedral arrangement of ligands in the high-spin states of the Fe(II), Co(II), and Ni(II) complexes (see Table
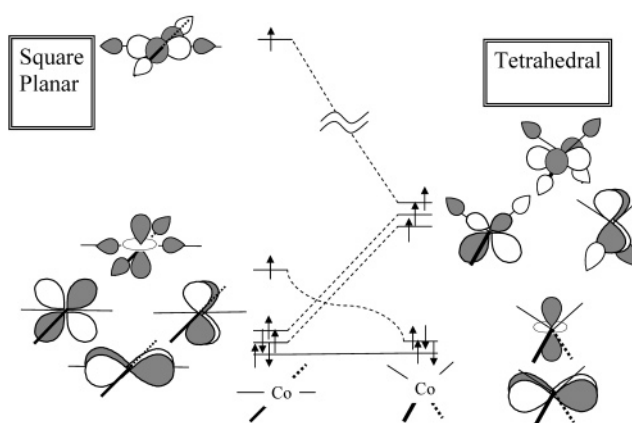

Figure 8. Walsh diagram for a tetrahedral to square planar conversion of a high-spin quartet Co(II)L$_4$ complex. The high-spin quintet state of the Fe(II) complex would have one less electron in the next to lowest of the depicted orbitals, whereas the high-spin triplet of the Ni(II) complex would have one additional electron in the middle or third level orbital. In all three high-spin cases the highest of these five orbitals is singly occupied.

1) can be understood on the basis of a Walsh diagram for the frontier orbitals[25] of a generalized M(II)L$_4$ complex (Figure 8). In this qualitative picture, the geometry of ML$_4$ systems is attributed in large part to the behavior of the highest of the singly occupied molecular orbitals (SOMOs). For the high-spin states, the energy of the highest SOMO is expected to rise dramatically as the tetrahedron is flattened due to increased antibonding character. This orbital is not occupied in the low-spin states, and the square planar structure is thus expected to be the more stable for the triplet Fe(II), doublet Co(II), and singlet Ni(II) complexes (see Table 1).

Alternatively, the Walsh diagram can be used to anticipate the spin states for scaffold enforced tetrahedral and square planar arrangements of ligands. In case of an enforced tetrahedral arrangement of ligands, Hund's rule would anticipate a high-spin configuration for the partially filled set of three degenerate orbitals (i.e., quartet state for d^7 Co-
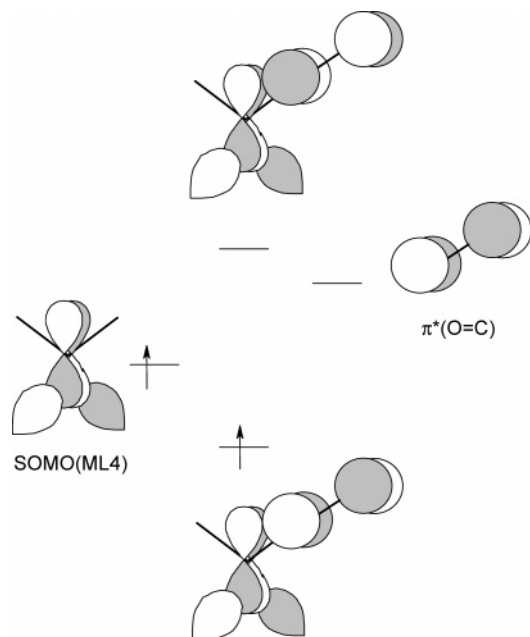
Computational Characterization of Metal Binding Groups

J. Chem. Theory Comput., Vol. 2, No. 4, 2006 **995**

Figure 9. Interaction diagram for $\pi^*(O=C)$ orbital of a π acceptor ligand and one of the metal SOMOs in a high-spin tetrahedral ML_4 complex. The energy gap between ligand π^*-$(O=C)$ orbital and $SOMO(ML_4)$ will determine the degree of stabilization of SOMO of the complex due to back-bonding. In Zn(II) complexes, the lower of the orbitals of the complex would be doubly occupied.

(II) complexes and a triplet state for d^8 Ni(II) complexes). On the other hand, a square planar arrangement of ligands would favor low-spin d^7 (i.e., doublet Co(II)) and d^8 (i.e., singlet Ni(II)) complexes.

The conformation of ligands about the metals in (PDF)M-(II)(BG) enzyme cocrystals is typically tetrahedral.[9] The framework of the enzyme itself probably plays a role in enforcing this geometry and increasing the likelihood that the metal ions are in a high-spin state.

Binding Trends across Metals. A qualitative understanding of the trends in the calculated enthalpies of water displacement across the spectrum of metals (Table 4 and Figure 5) can be offered in terms of traditional concepts of metal to carbonyl back-bonding. Figure 9 is an orbital diagram for the stabilizing back-bonding interaction expected between the SOMO of a tetrahedrally coordinated high-spin metal and the LUMO of a π-acceptor ligand (e.g., carbonyl group). This stabilizing interaction is expected to weaken in proceeding across the transition metals from Fe(II) to Co-(II) to Ni(II) due to the increasing energy gap between the $\pi^*(O=C)$ orbital and the SOMOs as the latter drop in energy. The weakening of this back-bonding interaction may account for the decreasing exothermicity for water displacement by π-acceptor ligands in the order

$$-\Delta H(\text{Fe(II)}) \approx -\Delta H(\text{Co(II)}) > -\Delta H(\text{Ni(II)})$$

Although the energy gap is expected to widen even further upon passing to Zn(II) complexes, the presence of two rather than one electron in this back-bonding HOMO of the complex may account for the reversal in the downward trend in binding strength.

Binding Trends across Ligands. Trends in the calculated reaction enthalpy across the spectrum of ligands listed in Table 4 can also be understood in terms of traditional bonding concepts. For example, the electron releasing property of a methyl group relative to a hydrogen atom can account for enhanced stability predicted for compound 2 relative to compounds 1 and 4. The alternate metal coordination scheme found acetylhydrazine complexes (compound 5), compared with complexes formed with the acetylhydroxylamine ligand (compound 4), can be attributed to a combination of enhanced basicity and decreased hydrogen bond acidity of an amino group relative to a hydroxyl group. The terminal amino group of the acetylhydrazine thus forms a dative bond with the metal, while the corresponding acetylhydroxylamine donates a hydrogen bond to the sulfide of the PATH ligand rather than interact with the metal. It is interesting that metal dependent shifts between bidentate and monodentate metal binding have been observed for the formate ligand in PDF. In iron and cobalt PDF, bidentate metal binding that involves both formate oxygens is observed, while in Zn PDF monodentate binding of one oxygen to the metal and hydrogen bonding of the other oxygen to the protein backbone is observed.[26]

It should be noted that the hydrogen bond predicted between the hydroxyl group of the hydroxamic acids and the basic sulfide of the PATH ligand in the (PATH)M(II)-(hydroxamic acid) complexes may not be present in the (PDF)M(II)(hydroxamic acid) complexes. In (PDF)M(II)-(hydroxamic acid) complexes, the hydroxyl group of a properly positioned hydroxamic acid can participate in a dative bond with the metal ion of the enzyme and simultaneously donate a hydrogen bond to a second base at the active site, which is not represented in our model system.

Despite the simplicity of our model system when compared with the actual (PDF)−Ni(II) active site, experimental measurements of PDF−Ni enzyme inhibition[5] are consistent with many of our results including the high binding strength calculated for the *N*-formylhydroxylamine (compound 1, Table 4) and hydroxamic acid (compound 4) and the relatively low binding strength calculated for the carboxylic acid (compound 3) and thiol (compound 6). On the other hand, the *N*-acetylhydrazine (compound 5), which we calculated to be the penultimate metal binder among the BGs studied, is 200 times less active as an enzyme inhibitor than the corresponding hydroxamic acid (compound 4).

Conclusions

Discovering an effective alternative to the hydroxamate metal binding group is a goal of both medicinal and crop protection research. The results discussed demonstrate the value density functional methods as a tool to be used in this quest. When coupled with qualitative molecular orbital reasoning about binding interactions, DFT calculations provide both insight and numbers that are of use in our exploration for alternative metal binding groups. The calculations are also sensitive in a meaningful way to the spin state of the metal at the binding site, a feature that may well be critical to ligand design and the understanding of biochemical inhibition assay results.

Supporting Information Available: Tables of geometric parameters for quartet (PATH)Co(II)Br (Table S1) and singlet (PATH)Zn(II)Br (Table S2) calculated at both the BP86/DGDZVP and B3LYP/DGDZVP levels. This material is available free of charge via the Internet at http://pubs.acs.org.

References

(1) Baldwin, B. C.; Corran, A. J.; Robson, M. J. *Pestic. Sci.* **1995**, *44*, 81−83.

(2) White, R. J.; Margolis, P. S.; Trias, J.; Yuan, Z. *Curr. Opin. Pharmacol.* **2003**, *3*, 502−507.

(3) Wu, C.-S.; Huang, J.-L.; Sun, Y.-S.; Yang, D.-Y. *J. Med. Chem.* **2002**, *45*, 2222−2228.

(4) Tobe, H.; Morishima, H.; Aoyagi, T.; Umezawa, H.; Ishiki, K.; Nakamura, K.; Yoshioka, T.; Shimauchi, Y.; Inui, T. *Agric. Biol. Chem.* **1982**, *46*, 1865−1872.

(5) Smith, H. K.; Beckett, R. P.; Clements, J. M.; Doel, S.; East, S. P.; Launchbury, S. B.; Pratt, L. M.; Spavold, Z. M.; Thomas, W.; Todd, R. S.; Whittaker, M. *Bioorg. Med. Chem. Lett.* **2002**, *12*, 3595−3599.

(6) Chen, D. Z.; Patel, D. V.; Hackbarth, C. J.; Wang, W.; Dreyer, G.; Young, D. C.; Margolis, P. S.; Wu, C.; Ni, Z.-J.; Trias, J.; White, R. J.; Yuan, Z. *Biochemistry* **2000**, *39*, 1256−1262.

(7) (a) Giglione, C.; Pierre, M.; Meinnel, T. *Mol. Microbiol.* **2000**, *36*, 1197−1205. (b) Jain, R.; Chen, D.; White, R. J.; Patel, D. V.; Yuan, Z. *Curr. Med. Chem.* **2005**, *12* (14), 1607−1621.

(8) (a) Dirk, L. M. A.; Williams, M. A.; Houtz, R. L. *Plant Physiol.* **2001**, *127*, 97−107. (b) Williams, M.; Hou, C.-X.; Dirk, L. M. A. *Abstract of Papers,* 227th ACS National Meeting, 2004; AGFD 41.

(9) Becker, A.; Schlichting, I.; Kabsch, W.; Groche, D.; Schultz, S.; Wagner, A. F. V. *Nat. Struct. Biol.* **1998**, *5*, 1053−1058.

(10) Madison, V.; Duca, J.; Bennett, F.; Bohanon, S.; Cooper, A.; Chu, M.; Desai, J.; Girijavallabhan, V.; Hare, R.; Hruza, A.; Hendrata, S.; Huang, Y.; Kravec, C.; Malcolm, B.; McCormick, J.; Miesel, L.; Ramamanathan, L.; Reichert, P.; Saksena, A.; Wang, J.; Weber, P. C.; Zhu, H.; Fischmann, T. *Biophys. Chem.* **2002**, *101−102*, 239−247.

(11) Apfel, C.; Banner, D. W.; Bur, D.; Dietz, M.; Hirata, T.; Hubschwerlen, C.; Locher, H.; Page, M. G. P.; Pirson, W.; Rosse, G.; Specklin, J.-L. *J. Med. Chem.* **2000**, *43*, 2324−2331.

(12) Clements, J. M.; Beckett, R. P.; Brown, A.; Catlin, G.; Lobell, M.; Palan, S.; Thomas, W.; Whittaker, M.; Wood, S.; Salama, S.; Baker, P. J.; Rodgers, H. F.; Barynin, V.; Rice, D. W.; Hunter, M. G. *Antimicrob. Agents Chemother.* **2001**, *45*, 563−570.

(13) Coats, R. A.; Lee, S. L.; Davis, K. A.; Patel, K. M.; Rhoads, E. K.; Howard, M. H. *J. Org. Chem.* **2004**, *69*, 1734−1737.

(14) (a) Howard, M. H.; Cenizal, T.; Gutteridge, S.; Hanna, W. S.; Tao, Y.; Totrov, M.; Wittenbach, V. A.; Zheng, Y.-J. *J. Med. Chem.* **2004**, *47*, 6669−6672. (b) Howard, M. H.; Cenizal, T. M.; Coats, R. A.; Samajdar, S. *Abstract of Papers,* 229th ACS National Meeting, 2005; AGRO 064. (c) Howard, M. H.; Cenizal, T. M.; Kucharczyk, R.; Samajdar, S. *Abstract of Papers,* 229th ACS National Meeting, 2005; AGRO 050.

(15) (a) Chang, S.; Karambelkar, V. V.; Sommer; R. D.; Rheingold, A. L.; Goldberg, D. P. *Inorg Chem.* **2000**, *41*, 239−248. (b) Chang, S.; Karambelkar, V. K.; diTargiani, R. C.; Goldberg, D. P. *Inorg. Chem.* **2001**, *40*, 194−195. (c) Chang, S.; Sommer, R. D.; Rheingold, A. L.; Goldberg, D. P. *Chem. Commun.* **2001**, 2396−2397. (d) Goldberg, D. P.; diTargiani, R. C.; Namuswe, F.; Minnihan, E. C.; Chang, S.; Zakharov, L. N.; Rheingold, A. L. *Inorg. Chem.* **2005**, *44*, 7559−7569.

(16) Frisch, M. J.; Trucks, G. W.; Schlegel, H. B.; Scuseria, G. E.; Robb, M. A.; Cheeseman, J. R.; Montgomery, J. A., Jr.; Vreven, T.; Kudin, K. N.; Burant, J. C.; Millam, J. M.; Iyengar, S. S.; Tomasi, J.; Barone, V.; Mennucci, B.; Cossi, M.; Scalmani, G.; Rega, N.; Petersson, G. A.; Nakatsuji, H.; Hada, M.; Ehara, M.; Toyota, K.; Fukuda, R.; Hasegawa, J.; Ishida, M.; Nakajima, T.; Honda, Y.; Kitao, O.; Nakai, H.; Klene, M.; Li, X.; Knox, J. E.; Hratchian, H. P.; Cross, J. B.; Adamo, C.; Jaramillo, J.; Gomperts, R.; Stratmann, R. E.; Yazyev, O.; Austin, A. J.; Cammi, R.; Pomelli, C.; Ochterski, J. W.; Ayala, P. Y.; Morokuma, K.; Voth, G. A.; Salvador, P.; Dannenberg, J. J.; Zakrzewski, V. G.; Dapprich, S.; Daniels, A. D.; Strain, M. C.; Farkas, O.; Malick, D. K.; Rabuck, A. D.; Raghavachari, K.; Foresman, J. B.; Ortiz, J. V.; Cui, Q.; Baboul, A. G.; Clifford, S.; Cioslowski, J.; Stefanov, B. B.; Liu, G.; Liashenko, A.; Piskorz, P.; Komaromi, I.; Martin, R. L.; Fox, D. J.; Keith, T.; Al-Laham, M. A.; Peng, C. Y.; Nanayakkara, A.; Challacombe, M.; Gill, P. M. W.; Johnson, B.; Chen, W.; Wong, M. W.; Gonzalez, C.; Pople, J. A. *Gaussian 03, revision B.04*; Gaussian, Inc.: Pittsburgh, PA, 2003.

(17) "B" is the Becke 88 gradient-corrected exchange functional: Becke, A. D. *Phys. Rev.* **1988**, *A38*, 3098−3100.

(18) "P86" is the Perdew 86 gradient-corrected correlation functional: Perdew, J. P. *Phys. Rev.* **1986**, *B33*, 8822−8824.

(19) (a) Becke, A. D. *J. Chem. Phys.* **1993**, *98*, 5648. (b) Lee, C.; Yang, W.; Parr, R. G. *Phys. Rev. B* **1988**, *37*, 785−789.

(20) (a) Dunlap, B. I. *J. Chem. Phys.* **1983**, *78*, 3140. (b) Dunlap, B. I. *J. Mol. Struct. (THEOCHEM)* **2000**, *529*, 37.

(21) Godbout, N.; Salahub, D. R.; Andzelm, J.; Wimmer, E. *Can. J. Chem.* **1992**, *70*, 560.

(22) Even now, relative energetics for transition-metal complexes is a very active topic. For example, see: Fouqueau, A.; Casida, M. E.; Daku, L. M. L.; Hauser, A.; Neese, F. *J. Chem. Phys.* **2005**, *122*, 044110/1−13.

(23) For example, see: Himo, F.; Siegbahn, P. E. M. *Chem. Rev.* **2003**, *103*, 2421−2456.

(24) Dobbs, K. D.; Dixon, D. A. *J. Phys. Chem.* **1996**, *100*, 3965−3973. Also, B3LYP/DGDZVP structures for quartet (PATH)-Co(II)Br and singlet (PATH)Zn(II)Br are compared with BP86/DGDZVP and experimental structures in Supporting Information Tables S1 and S2.

(25) Albright, T. A.; Burdett, J. K.; Whangbo, M.-H. *Orbital Interactions in Chemistry*; John-Wiley and Sons: New York, 1985; Chapter 19: The ML_2 and ML_4 Fragments, pp 358−380.

(26) Jain, R.; Hao, B.; Liu, R.-p.; Chan, M. K. *J. Am. Chem. Soc.* **2005**, *127*, 4558−4559.

CT050192U